Rock and Soil Mechanics

Volume 44 | Issue 2 Article 8

4-10-2023

# Effects of lead contamination on macro-water retention and micro-structural evolution of loess

Shao-jie WEN
*School of Civil Engineering, Xi'an University of Architecture and Technology, Xi'an, Shaanxi 710055, China, Shaanxi Key Laboratory of Geotechnical and Underground Space Engineering, Xi'an University of Architecture and Technology, Xi'an, Shaanxi 710055, China*

Wen-chieh CHENG
*School of Civil Engineering, Xi'an University of Architecture and Technology, Xi'an, Shaanxi 710055, China, Shaanxi Key Laboratory of Geotechnical and Underground Space Engineering, Xi'an University of Architecture and Technology, Xi'an, Shaanxi 710055, China*

Wen-le HU
*School of Civil Engineering, Xi'an University of Architecture and Technology, Xi'an, Shaanxi 710055, China, Shaanxi Key Laboratory of Geotechnical and Underground Space Engineering, Xi'an University of Architecture and Technology, Xi'an, Shaanxi 710055, China*

Rock and Soil Mechanics 2023 44(2): 451−460 ISSN 1000−7598
https: //doi.org/10.16285/j.rsm.2022.5239 http://rocksoilmech.researchcommons.org/journal

# Effects of lead contamination on macro-water retention and micro-structural evolution of loess

WEN Shao-jie[1, 2], CHENG Wen-chieh[1, 2], HU Wen-le[1, 2]

1. School of Civil Engineering, Xi'an University of Architecture and Technology, Xi'an, Shaanxi 710055, China

2. Shaanxi Key Laboratory of Geotechnical and Underground Space Engineering, Xi'an University of Architecture and Technology, Xi'an, Shaanxi 710055, China

**Abstract:** The physical and chemical reactions between heavy metals in landfill leachate and soil may change the microstructure of soil, then the diffusion and migration of heavy metals and other toxic substances, threaten human health and surrounding environment. In order to investigate the effects of heavy metal contamination on macroscopic water retention and microstructure of loess, the soil-water characteristic curves of Pb-contaminated loess were measured by axial translation technique. Characterization of mesoscopic structure changes was clarified by scanning electron microscopy (SEM), mercury injection (MIP), X-ray diffraction (XRD) and Zeta potential. The results show that the air-entry values of Pb-contaminated loess decrease with the increase of Pb-concentration. When the lead pollution concentration increases from 0 mg/kg to 2 000 mg/kg, the air-entry values decrease from 19.18 kPa to 12.12 kPa, indicating that lead contamination lead to a decrease in water retention. On the contrary, the permeability increases with the increase of lead concentrations. The saturated permeability coefficient increases from $7.92\times10^{-8}$ m/s to $3.73\times10^{-7}$ m/s. The physicochemical reaction and reduction of Zeta potential caused by lead contamination produce flocculation structure, and the proportion of small pores decreases while that of medium pores increases. The microscale structural evolution has a good correspondence, induced by the lead contamination, with macroscopic water retention capacity and permeability. The results can provide important parameters for the study of unsaturated seepage and solute transport in heavy metal contaminated sites.

**Keywords:** contaminated soil; heavy metal; micro-structure; soil-water characteristic curve; matrix suction; permeability properties

## 1 Introduction

A large amount of domestic waste is generated every day with the accelerated urbanization process. And sanitary landfill gradually become the main choice for municipal solid waste disposal in various countries because of simple operation, low cost, and large disposal capacity[1]. Due to the improper waste classification and disposal, the landfill leachate contains many toxic substances. When the leachate leaks and infiltrates into the underground environment, the heavy metals in the leachate are adsorbed on the soil particles through chemical adsorption or cation exchange, then the metallic bond will be formed with the aggregates[2−3]. Zha et al.[4] found that the pore size between the flocculation structure and aggregates increased with the increase of heavy metal concentration, while the unconfined compressive strength decreased. Li et al.[2] and Dutta et al.[5] revealed that soil permeability increased with the increase of heavy metal concentration. Zhang et al.[3] analyzed the influence of $Cu^{2+}$ contamination on the microstructure and permeability of clay, and they concluded that the change of inner pore size of clay, caused by $Cu^{2+}$, makes a difference in macroscopic permeability. The soil microstructure change by heavy metal affects the long-term stability of the impermeable liner in landfill, then toxic and harmful substances migrate into the environment with the leachate[3]. The migrating and leaching processes of contaminants are usually the strict unsaturated fluid migration phenomenon[6].

Soil-water characteristic curve (SWCC) is used to characterize the relationship between suction and water retention, it is the basis for investigating seepage and solute transport in unsaturated soil[6]. The SWCC of soil is mainly affected by pore size distribution, soil particle size distribution, density, clay content, etc.[6−7]. Many scholars have established the relationship between pore size distribution and SWCC. For example, Simms et al.[8] proposed a model to predict SWCC by using pore size distribution, where pore shrinkage was considered. Fei et al.[9] improved the prediction method of SWCC based on pore size distribution of soil, which can obtain the result conveniently and accurately. The microstructure of soil plays a decisive role in the soil properties[10−11]. Qi et al.[11] explained the water retention characteristics of expansive soil under the hydrating path from the microscopic mechanism. In addition, Li et al.[12] and Li et al.[13] fitted the soil-water characteristic curve using the frequently-used SWCC models, and analyzed the water retention characteristics. Zhang et al.[14] examined the deformation and water retention characteristic of loess in hydrating process, and proposed a modified V-G model by considering the void ratio change. However, few studies focus on the effects of heavy metal contamination on water retention characteristic.

$Q_3$ loess was taken as the research object in this

Received: 03 March 2022 Accepted: 29 August 2022
This work was supported by the Youth Program of the Organization Department of the Central Committee of the CPC "National Overseas High-level Talents Introduction Program" (2019).
First author: WEN Shao-jie, male, born in 1992, Doctoral students, research interests: environmental geotechnical engineering. E-mail: wenshaojie@xauat.edu.cn.

paper, the soil-water characteristic curve and permeability of Pb-contaminated loess were investigated by means of multi-step overflow method, and the water retention ability and permeability characteristics of Pb-contaminated loess were analyzed. Meanwhile, scanning electron microscope (SEM), mercury intrusion porosimetry (MIP), X-ray diffraction (XRD) and Zeta potential test were employed to observe the microstructure of Pb-contaminated soil, and the influences of heavy metal on macroscopic water retention and permeability characteristics were clarified from the microscopic level. It is expected to provide useful reference for the construction and treatment of heavy metal contaminated sites.

## 2 Materials and methods

### 2.1 Materials

$Q_3$ loess used in this test is collected at 3–4 m depth. According to "*Standard for geotechnical testing method*" (GB/T 50123-2019)[15] and the unified soil classification system[16], its basic physico-chemical properties were measured through laboratory tests, as shown in Table 1, and the particle size distribution curve is presented in Fig. 1. Since lead contamination threatened to the surrounding environment and human health[17], lead nitrate ($Pb(NO_3)_2$) was selected as the main contaminant for Pb-contaminated specimens.

**Table 1 Physico-chemical properties of $Q_3$ loess**

| Particle distribution /% | | | Void ratio | Unit weight | Specific gravity | Natural water content | Liquid limit $w_L$ | Plastic limit $w_P$ | Classification symbol | Relative content of chemical element /% | | | | | | |
|---|---|---|---|---|---|---|---|---|---|---|---|---|---|---|---|---|
| Sand | Silt | Clay | | /(kN • m$^{-3}$) | $G_s$ | /% | /% | /% | | Si | Ca | Mg | Na | K | Fe | Al |
| 3.3 | 87.4 | 9.3 | 0.898 | 16.2 | 2.69 | 16.5 | 31.6 | 19.5 | CL | 25.45 | 11.82 | 1.59 | 0.87 | 2.69 | 4.99 | 7.00 |

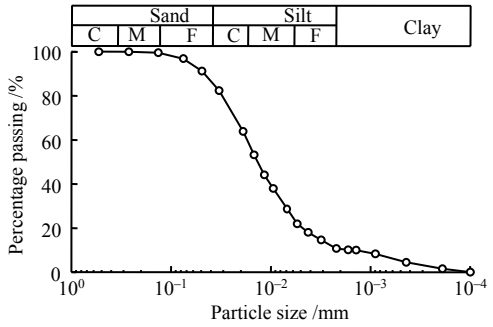


**Fig. 1 Particle-size distribution curve of $Q_3$ loess**

### 2.2 Specimen preparation

In order to obtain contaminated soil specimens with relatively uniform contamination degree, Pb-contaminated loess specimens were prepared in the laboratory by static pressure method to avoid the difference caused by the uneven pore structure of undisturbed soils. The loess was crushed and sieved using 2 mm sieve, and then it was dried for 24 hours at 105 °C. Four contamination concentrations were set with reference to the common contamination degree of sites, and the mass ratios of lead ion to dry soil were 0, 500, 1 000 and 2 000 mg/kg[4]. A certain amount of loess, $Pb(NO_3)_2$ and deionized water were weighed, respectively. $Pb(NO_3)_2$ was dissolved in deionized water, and the solution was mixed with the corresponding proportion of loess, then stewed for 24 hours. The soil specimens were compacted into the mold in three layers, meanwhile, the height of each layer was controlled to obtain Pb-contaminated specimens with a diameter of 39.1 mm, a height of 40 mm, a dry density of 1.4 g/cm$^3$ and a water content of 16%. Compared with the conventional triaxial specimen (39.1 mm in diameter and 80 mm in height), the specimen height was reduced to 40 mm, thus the time required for suction balance became short[18]. After vacuum saturation with deionized water, the prepared specimens were sealed and placed in a constant temperature and humidity curing box for 10 days, with a temperature of (20±2) °C, and a relative humidity of 95%, so that lead ions distribute uniformly in the loess[4].

### 2.3 Instruments and methods

The British VJ Tech VJT9030 unsaturated triaxial apparatus was employed in this test, which mainly consists of double wall cell, confining pressure controller and volume change device, reverse pressure controller, air pressure controller and data acquisition system. Based on the axial translation technique, the multi-step overflow method was adopted to conduct the SWCC test in a dehydrating path, as shown in Fig. 2. The bottom of the specimen was always close to the ceramic plate during the test, and the air pressure gradually increased at the top of the specimen to improve the matric suction. As the water in the specimen flowed to the reverse pressure controller through the ceramic plate under the action of air pressure, the water outflow $\Delta Q$ was monitored by the reverse pressure controller in real time. When water outflow $\Delta Q$ tended to be stable, the matric suction reached equilibrium, and then the air pressure increased to the next level. The double wall cell and volume change device can measure the volume change of the specimen in dehydrating process in real time, and the saturation degree can be further calculated. The test parameters are shown in Table 2. After the test, the specimens were taken out to measure the water content. According to the overflow volume at each pressure stable stage, the relationship between the matric suction and the saturation degree or volumetric water content can be obtained in the whole process.

GDS permeameter was employed to conduct saturated permeability test, and the leachate was collected for cation concentration test. JSM-7610F scanning electron microscope was used to observe the microstructure characteristics of Pb-contaminated loess, and the microstructure information such as pore size distribution and pore number were extracted by Image-Pro Plus 6.0 software. Bruker AXS X-ray diffractometer was used to analyze the phase composition change of Pb-contaminated loess. The soil specimen was fully ground into powder and sieved using 0.075 mm. Step scanning was selected during the test. The scanning speed and step width were set to 2 (°)/min and 0.02°, respectively. AutoPore Iv 9500 automatic mercury intrusion porosimeter was used to analyze the pore size distribution of Pb-contaminated loess, and the middle part of the soil specimen was selected to cut into a cube with size of 1 $cm^3$. In order to avoid the pore structure change of the specimen in drying process, the freeze-drying technique was used to process and weigh the specimen. Malvern Zetasizer Nano ZS90 Zeta potential analyzer was employed to analyze the Zeta potential change of Pb-contaminated loess. The soil specimen was fully ground into powder, and dispersant (water) was added into the powder to make a suspension for testing Zeta potential.

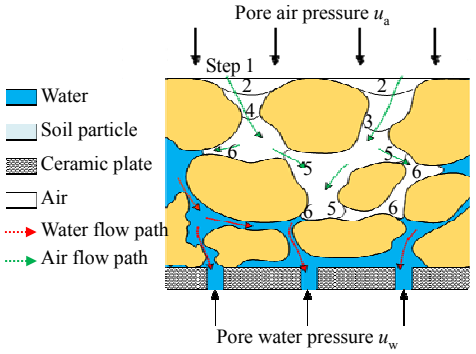


**Fig. 2 Diagram of multi-step overflow method**

**Table 2 Parameters applied to the permeability tests**

| Specimen | Contamination concentration /(mg • $kg^{-1}$) | Effective confining pressure /kPa | Pore air pressure /kPa | Pore water pressure /kPa | Matric suction /kPa |
|---|---|---|---|---|---|
| 1 | 0 | 50 | 30, 35, 50, 90, 150, 230, 330 | 30 | 0, 5, 20, 60, 120, 200, 300 |
| 2 | 500 | 50 | 30, 35, 50, 90, 150, 230, 330 | 30 | 0, 5, 20, 60, 120, 200, 300 |
| 3 | 1 000 | 50 | 30, 35, 50, 90, 150, 230, 330 | 30 | 0, 5, 20, 60, 120, 200, 300 |
| 4 | 2 000 | 50 | 30, 35, 50, 90, 150, 230, 330 | 30 | 0, 5, 20, 60, 120, 200, 300 |

## 3 Results and analysis

### 3.1 Soil-water characteristic curve

It is time-consuming to obtain the data of matric suction and saturation degree, which are indispensable to evaluate the water retention ability. Therefore, the soil-water characteristic curve models are used for parameter fitting, so that the continuous function is obtained. The frequently-used models are as follows:

Gardner model (GA model)[19]:

$$S_{eL} = S_{rL} + \frac{S_L - S_{rL}}{1 + (s/a)^n} \tag{1}$$

Fredlund & Xing model (FX model)[20]:

$$S_{eL} = S_{rL} + \frac{S_L - S_{rL}}{\left\{\ln\left[e + (s/a)^n\right]\right\}^m} \tag{2}$$

Van Genuchten model (VG model)[21]:

$$S_{eL} = S_{rL} + \frac{S_L - S_{rL}}{\left[1 + (s/a)^n\right]^m} \tag{3}$$

where $S_{eL}$ is the effective saturation degree; $S_L$ is the saturation degree (%); $S_{rL}$ is the residual saturation degree (%); $s$ is the matric suction (kPa); $a$ is a parameter related to the air-entry value (kPa); $n$ is a parameter related to the dehydrating rate of soil when the matric suction is greater than the air-entry value; $m$ is a parameter related to residual water content[13, 22–23]; and natural constant $e = 2.718\ 28$.

The data with contamination concentration of 1 000 mg/kg is selected as an example to do the parameter fitting based on FX model, GA model, and VG model, as shown in Fig. 3. The three models can well fit the soil-water characteristic curve of Pb-contaminated loess within the test range. The GA model is simple with few input parameters and relatively low fitting degree $R^2$. The fitting degrees $R^2$ of FX model and VG model are above 0.99, while the predicted values of the two models are significantly different beyond the test range. For Pb-contaminated soil with different concentrations, the fitting parameters of the three models are shown in Table 3. According to the fitting results, VG model and FX model well fit the Pb-contaminated soil with different concentrations within the test range (matric suction less than 300 kPa).

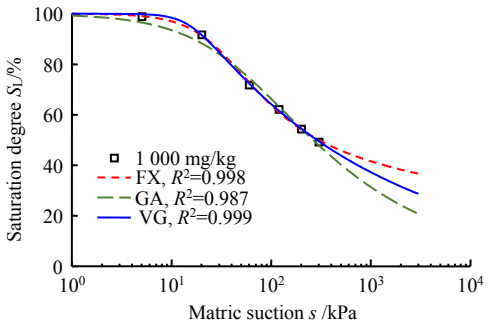


**Fig. 3 Results of curve fitting using FX, GA, and VG models**

**Table 3 Fitting parameters for FX, GA, and VG models**

| Concentration /(mg·kg$^{-1}$) | SWCC model | Parameter $a$ /kPa | Parameter $n$ | Parameter $m$ | $R^2$ |
|---|---|---|---|---|---|
| 0 | FX | 32.76 | 0.32 | 2.32 | 0.999 |
| | GA | 104.21 | 0.43 | — | 0.979 |
| | VG | 22.09 | 3.30 | 0.06 | 0.998 |
| 500 | FX | 30.68 | 0.44 | 1.88 | 0.997 |
| | GA | 74.30 | 0.43 | — | 0.985 |
| | VG | 18.89 | 3.25 | 0.07 | 0.999 |
| 1 000 | FX | 26.02 | 0.47 | 1.75 | 0.998 |
| | GA | 53.27 | 0.39 | — | 0.987 |
| | VG | 15.42 | 3.26 | 0.07 | 0.999 |
| 2 000 | FX | 24.93 | 0.51 | 1.63 | 0.998 |
| | GA | 46.47 | 0.38 | — | 0.990 |
| | VG | 15.69 | 2.40 | 0.10 | 0.998 |

Cai et al.[24] reported that the VG model can well fit the high suction part of SWCC of sandy loess. Since the maximum suction measured by the multi-step overflow method is 300 kPa in this test, VG model is finally adopted to obtain the high suction part of SWCC, and the water retention ability and permeability are also evaluated.

Based on the axial translation technique, the multi-step overflow method is used to obtain the soil-water characteristic curve against different $Pb^{2+}$ concentrations in dehydrating path, as shown in Fig. 4. The saturation degree $S_L$ decreases gently at the initial stage within the test range, while decreases rapidly with the increase of suction $s$. Meanwhile, the $S_L$–$s$ curve shifts downward with the increase of $Pb^{2+}$ concentration, indicating that lead contamination reduces the saturation degree of loess under the same matric suction.

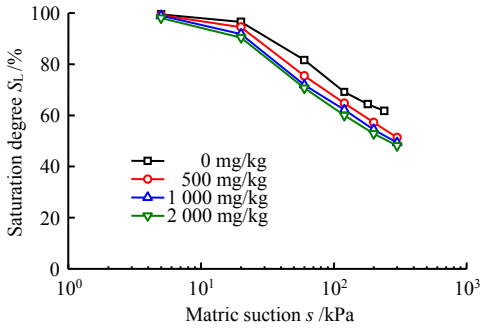


**Fig. 4 Soil-water characteristic curves against different $Pb^{2+}$ concentrations**

The measured data of soil-water characteristic curve against different $Pb^{2+}$ concentrations were analyzed using VG model, as shown in Fig. 5. With the increase of $Pb^{2+}$ concentration, the suction value at the inflection point of the fitting curve decreases gradually, in other words, the air-entry value of the saturated specimen decreases. When the $Pb^{2+}$ concentration increases from 0 mg/kg to 500, 1 000, and 2 000 mg/kg, the air-entry value of saturated specimen decreases from 19.18 kPa to 16.24, 12.75, and 12.12 kPa. The matric suction and air-entry value decrease with the increase of $Pb^{2+}$ concentration, indicating that lead contamination reduces the water retention ability of loess.

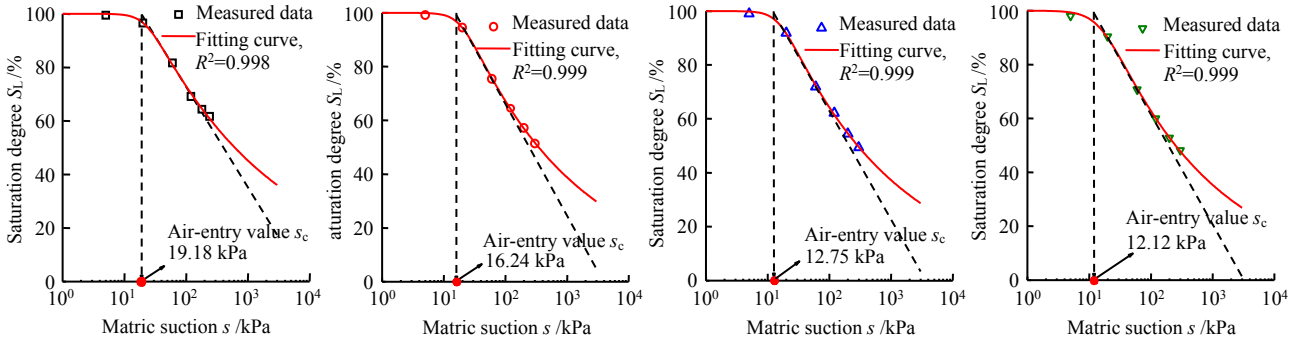


(a) $Pb^{2+}$ concentration of 0 mg/kg (b) $Pb^{2+}$ concentration of 500 mg/kg (c) $Pb^{2+}$ concentration of 1 000 mg/kg (d) $Pb^{2+}$ concentration of 2 000 mg/kg

**Fig. 5 Fitting curves of the VG model**

### 3.2 Prediction of permeability coefficient curve

Because of the long experiment period, complicated operation, and immature existing technique, it is difficult to ensure the measuring precision reliability of permeability coefficient of unsaturated soil. Many scholars[12−13] adopted Childs & Collis-Geroge model (CCG model) to indirect predict the permeability coefficient of unsaturated soil based on the soil-water characteristic curve:

$$k_L(\theta_L)_i = \frac{k_s}{k_{sc}} A_d \sum_{j=i}^{m} [(2j+1-2i)(u_a-u_w)_j^{-2}], \quad i=1,\cdots,m \tag{4}$$

$$A_d = \frac{T_s^2 \rho_L g}{2\mu_L} \frac{\theta_L^p}{N^2} \tag{5}$$

$$k_{sc} = A_d \sum_{j=i}^{m} [(2j+1-2i)(u_a-u_w)_j^{-2}], \quad i=0,1,2,\cdots,m \tag{6}$$

where $(u_a-u_w)_j$ is the matric suction corresponding to the midpoint of the $j$-th interval; $k_s$, $k_{sc}$, and $k_L(\theta_L)_i$ are the saturated permeability coefficient, calculated saturated permeability coefficient, and the unsaturated permeability coefficient (m/s), respectively; $T_s$ is the surface tension of water (kN/m); $\mu_L$ is the absolute viscosity of water (N·s/m$^2$); $\rho_L$ is the water

density (kg/m$^3$); $g$ is gravitational acceleration (m/s$^2$); $p$ is the interaction coefficient of pores with different sizes, and $p=2$; $\theta_L$ is the saturated volumetric water content (%); $N$ is the total number of calculated intervals between saturated volumetric water content and residual volumetric water content; $i$ is the interval number; and $j$ is the count from $i$ to $m$, taking $m=20$.

Based on the fitting results of VG model, the permeability coefficients of compacted loess are predicted by CCG model against different lead contamination concentrations, as shown in Fig. 6. The permeability coefficients of loess against different contamination concentrations decrease with saturation degree. During the process from saturation to drying, soil pores exist in three different states: liquid, gas-liquid coexistence and gas. The connectivity of pore fluid is good in high saturation degree, so do as the permeability coefficient. Gas-liquid channels exist with the decrease of saturation degree, which leads to a significant decrease in the connectivity of pore fluid, then the highly tortuous liquid channels form, and permeability coefficient decreases rapidly. The higher the contamination concentration, the greater the corresponding permeability coefficient is. When the contamination concentration increases from 0 mg/kg to 2 000 mg/kg, the saturated permeability coefficient increases from $7.92\times10^{-8}$ m/s to $3.73\times10^{-7}$ m/s. The main reason for this is that the clay particles are negatively charged, and lead reacts with them in adsorption and ion exchange form, which results in the reduction of the diffuse double layer thickness and the increase of the minimum capillary diameter (the relevant explanation of the capillary diameter increasing will be discussed later in this paper). Thus the soil pore structure is varied, causing the change of permeability characteristics.

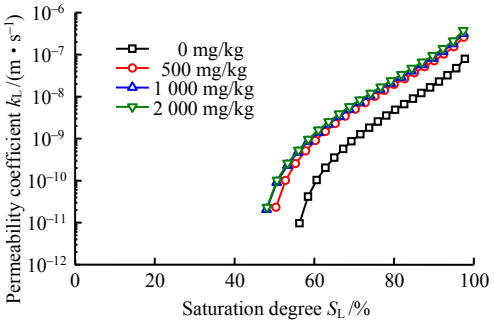


**Fig. 6 Relationships of permeability coefficient versus saturation against different $Pb^{2+}$ concentrations**

Figure 7 presents the relationship between loess permeability coefficient and matric suction against different $Pb^{2+}$ concentrations. The permeability coefficient of Pb-contaminated loess decreases with the increase of matric suction, and its decrease rate increases with the increase of lead concentration. Pore water is gradually replaced by air with increasing matric suction, and the flow channel of liquid becomes narrow or blocked, resulting in the increasing of the liquid tortuosity and the decreasing of the permeability coefficient. Lead contamination further reduces the water retention ability of loess and shows a lower saturation degree under the same matric suction (see Fig. 4). Therefore, the decrease rate of permeability coefficient of Pb-contaminated loess is significantly accelerated with the increase of matric suction.

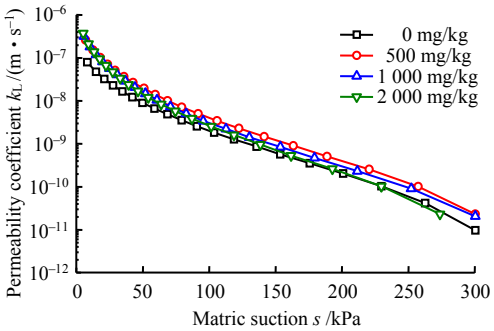


**Fig. 7 Relationships of permeability coefficient versus matric suction against different $Pb^{2+}$ concentrations**

### 3.3 Microscopic test results and analysis

3.3.1 Diffuse double layer model

The macro phenomenon is analyzed from the view of microstructure by combining with the theoretical model of the diffuse double layer (DDL) in this section. The negative charge of clay mineral form an electric field around it, then the adsorbed water molecules (polar molecules) and cations in solution arrange on soil particle surface orderly, as shown in Fig.8. According to $\zeta$–$X$ curve, the electrostatic attraction is the strongest near the soil particle surface, and the hydrated cation and the cation in aqueous solution are firmly adsorbed on the surface of soil particles to form a fixed layer (Stern layer). As the distance $X$ increases, the electrostatic attraction decreases, thus the electrostatic attraction constraints on the hydrated ion and the cation in the aqueous solution decrease, and their activity is greater than in the fixed layer, forming a diffusion layer (Gouy layer). With the further increase of distance $X$, the aqueous solution is no longer affected by the negative charge

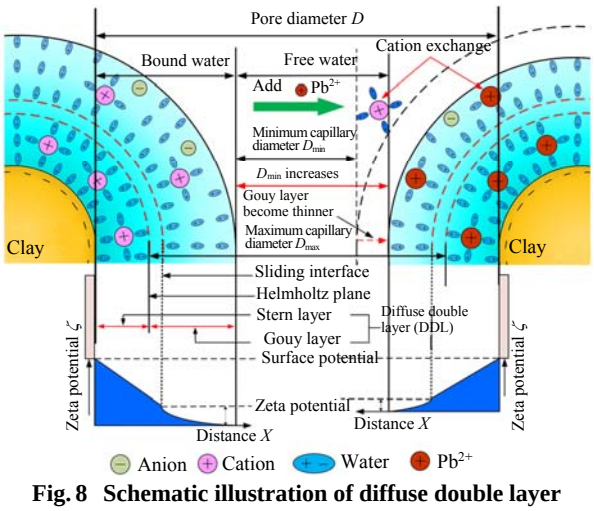


**Fig. 8 Schematic illustration of diffuse double layer**

on soil particle surface, and its state belongs to Brownian motion, which can be regarded as free water.

The diffuse layer thickness depends not only on the charge density of the mineral surface, but also on the ionic properties, valence, pH value and ionic concentration in the aqueous solution. Higher cation valence in the aqueous solution leads to stronger electrostatic attraction between the cation and the soil particle, then the hydration molecules and cations are less required to balance the negative charge on the soil particle surface, and the diffuse layer becomes thinner. As shown in Fig. 9, the absolute value of the electro kinetic potential $\zeta$ decreases with the increase of $Pb^{2+}$ concentration, and the negative potential on the soil particle surface decreases from –15.7 mV to –11.2 mV. The heavy metal cations increase the concentration and valence of cations in the pore fluid, then the negative charge on soil particle surface are neutralized, leading to a reduction in the negative potential on soil particle surface, and the Gouy layer becomes thinner. At this moment, the van der Waals attraction between particles becomes greater than the repulsion force, the clay particles aggregate, forming an agglomerated structure[25], thus the pore channels are widened. On the other hand, thinner Gouy layer thickness increases the minimum capillary diameter $D_{min}$ between the free interfaces of two soil particles, and some pore fluid channels are produced. The Pb-contaminated soil exhibits the enhancement of the permeability and the reduction of the air-entry value and the water retention ability on macroscopic scale (see Figs. 5 and 6).

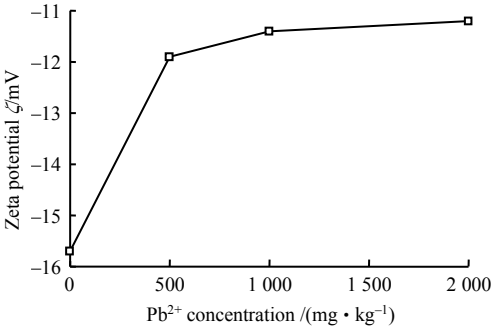


**Fig. 9 Influence of $Pb^{2+}$ concentration on $\zeta$ potential of loess**

3.3.2 SEM results and analysis

Image-Pro Plus 6.0 software is used for binarization and microstructure parameter acquisition of SEM images, as shown in Fig. 10. According to the classification method of loess pore in Lei[26]: the micro pore diameter is less than 2 μm, the small pore diameter ranges from 2 to 8 μm, the meso pore diameter ranges from 8 to 32 μm, and the large pore diameter is larger than 32 μm, then microscopic pore parameters are collected. The SEM images with a magnification of 500 times are selected for microstructure analysis, as shown in Fig. 11. We can identify the pore structure (including intergranular pores and intragranular pores) of Pb-contaminated loess and the aggregation structure caused by lead contamination from the original image. It can be seen that the size and content of intergranular pores increase with the increase of contamination concentration. Zhang et al.[3] found that the soil particles tend to be a condensed structure after adsorbing $Cu^{2+}$. Figure 12 illustrates the proportion of four kinds of pores against different $Pb^{2+}$ concentrations. The proportion of meso pores in loess increases with the increase of $Pb^{2+}$ concentration, while those of micro pores and small pores decrease. When the contamination concentration increases from 0 mg/kg to 500, 1 000, and 2 000 mg/kg, the proportion of micro pore decreases from 37.91% to 29.55%, 19.01% and 15.13%, respectively, and that of meso pore increases from 17.32% to 34.65%, 32.7%, and 53.31%, respectively. With the increase of $Pb^{2+}$ concentration in pore fluid, $Pb^{2+}$ enters the diffuse double layer of clay particles under the action of potential energy and electrostatic attraction, thereby the number of cations or hydrated ions is less required to balance the negative charge on soil particle surface, and the Gouy layer becomes thinner (see Fig. 8), which reduces the repulsion force between clay particles, and increases the van der Waals attraction, and consequently, clay particles aggregate, and larger pore channels form[2, 25]. The proportion of small pores and micro pores decreases, while that of meso pores increases, then the water retention ability of Pb-contaminated loess decreases, leading to a higher water loss rate and a smaller air-entry value, thus the decrease rate of permeability coefficient of Pb-contaminated loess become faster with the increase of matric suction (see Fig. 7).

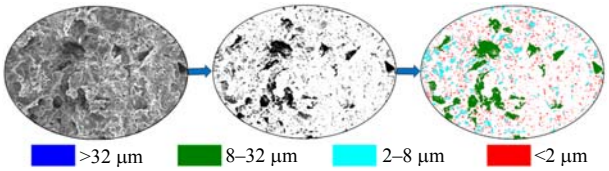


**Fig. 10 Procedures of the SEM images binarization process**

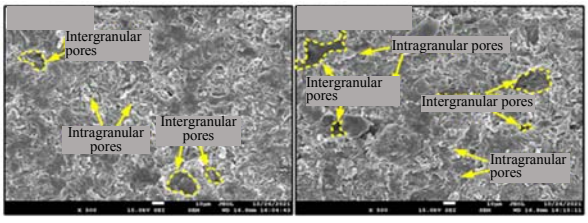


(a) $Pb^{2+}$ concentration 0 mg/kg (b) $Pb^{2+}$ concentration 500 mg/kg

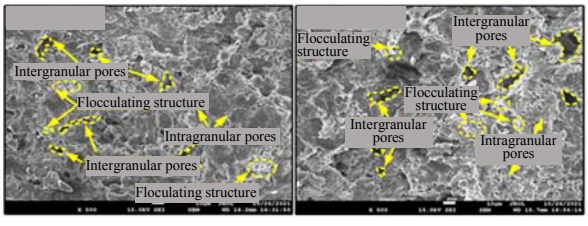


(c) $Pb^{2+}$ concentration 1 000 mg/kg (d) $Pb^{2+}$ concentration 2 000 mg/kg

**Fig. 11 SEM images against different $Pb^{2+}$ concentrations**

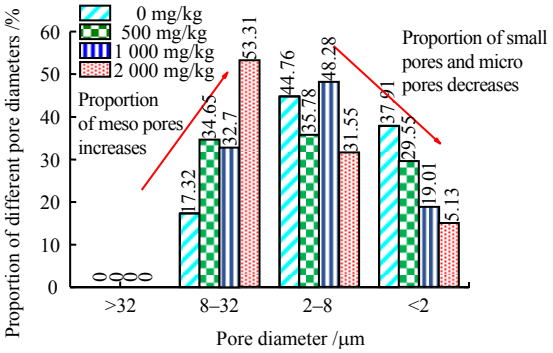


**Fig. 12 Proportion of four kinds of pores against different $Pb^{2+}$ concentrations**

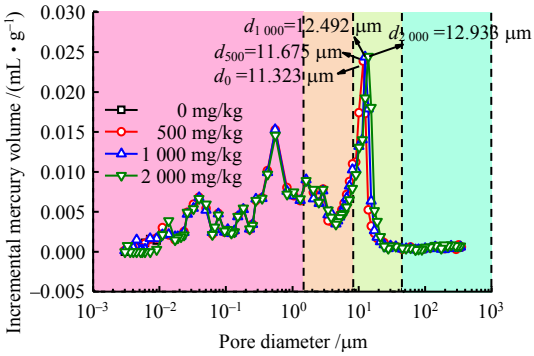


**Fig. 13 Incremental pore volume curves**

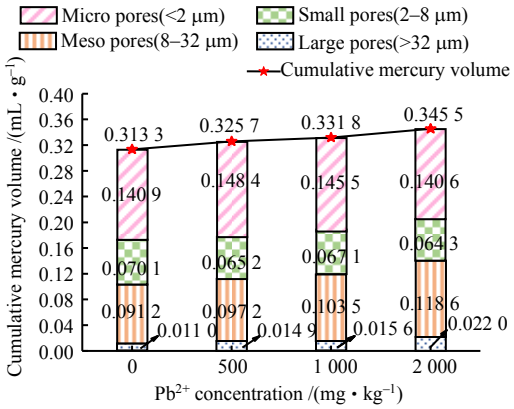


**Fig. 14 Distribution of four pore categories against different $Pb^{2+}$ concentrations**

3.3.3 MIP results and analysis

The incremental pore volume curves of loess specimens are obtained from the MIP test against different $Pb^{2+}$ concentrations, as shown in Fig. 13. There are two peaks in the pore distribution curve of Pb-contaminated compacted loess, where one peak corresponds to the dominant pore size of intragranular pores, and the other peak corresponds to that of intergranular pores. The results indicate that the pore size of intergranular pores changes from 11.323 μm increased to 11.675, 12.492, 12.933 μm with the increase of $Pb^{2+}$ concentration, which is consistent with that in literature [2]. Figure 14 presents the pore size distribution of four kinds of pores. The proportion of large pores and meso pores increases with the increase of $Pb^{2+}$ concentration. When the concentration increases from 0 mg/kg to 500, 1 000, and 2 000 mg/kg, the cumulative mercury volume increases from 0.313 3 mL • $g^{-1}$ to 0.325 7, 0.331 8, and 0.345 5 mL • $g^{-1}$, indicating that the pore structure of the specimen has changed from closed or semi-closed pores to more open pores. Flocculation may occur due to the reduction of the diffuse double layer thickness caused by $Pb^{2+}$, and the aggregation of particles tends to change the proportion of large pores, causing an increase in pore diameter between particles[2]. These results are basically consistent with the SEM: the proportion of micro pores decreases with the increase of $Pb^{2+}$ concentration, while that of meso pores increases.

3.3.4 XRD results and analysis

The XRD results of Pb-contaminated loess against different concentrations are shown in Fig. 15. It indicates that the main minerals in loess are quartz, calcite, albite, illite, orthoclase and kaolinite. Lead contamination reduces the diffraction peak intensity of main minerals in loess, it is mainly because of the disintegration and transformation of minerals caused by lead contamination. Wu et al.[27] believed that clay minerals have the characteristics of adsorbing cations and keeping them in an exchange state. Illite and kaolinite in loess absorb and exchange with lead ions[28–29]:

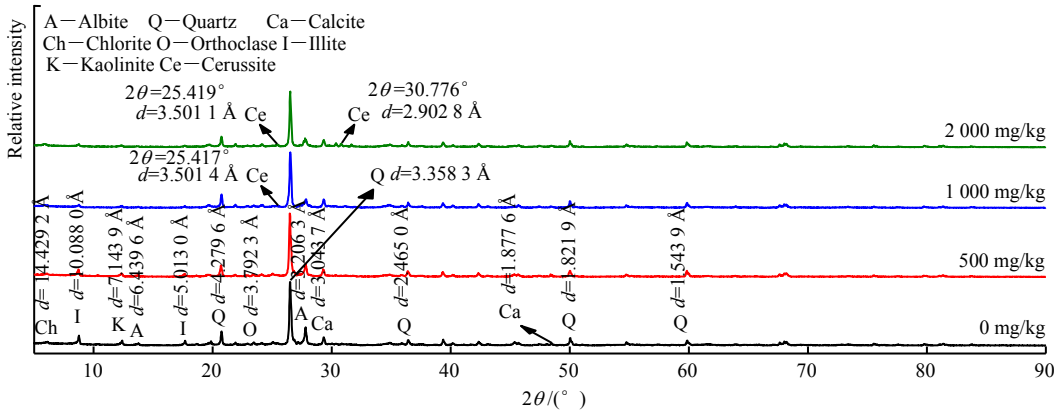


**Fig. 15 XRD test results of the Pb-contaminated loess**

$$2\equiv SOK+Pb^{2+}\longrightarrow \equiv SOPbOS\equiv +2K^{+} \quad (7)$$

$$2\equiv SOH+Pb^{2+}\longrightarrow \equiv SOPbOS\equiv +2H^{+} \quad (8)$$

In addition, lead ions lead to the increase of interlayer space of main minerals in loess. For example, the interlayer space of illite increases from 10.088 0 Å to 10.108 8 Å, albite increases from 3.206 3 Å to 3.208 6 Å, orthoclase increases from 3.792 3 Å to 3.795 3 Å, and kaolinite increases from 7.143 9 Å to 7.155 9 Å, which is similar to the results of Li et al.[2]. The reason may be that lead ion reduces the diffuse double layer thickness of clay particles. New minerals are found in Pb-contaminated loess at 25.419° and 30.776°, such as cerussite ($PbCO_3$), which is mainly because of the ion exchange reaction between calcite, dolomite and $Pb^{2+}$ in loess:

$$CaCO_3(s)+Pb^{2+}\longrightarrow Ca^{2+}+PbCO_3(s) \quad (9)$$

$$CaMg(CO_3)_2(s)+2Pb^{2+}\longrightarrow Ca^{2+}+Mg^{2+}+PbCO_3(s) \quad (10)$$

3.3.5 Cation concentration of leachate

It is generally believed that the cation exchange reaction is affected by the ionic valence, radius and relative content[28]. According to the exchange capacity of different cations, the cations ($Na^+$, $K^+$, $Ca^{2+}$, $Mg^{2+}$) in the minerals react with lead ions by cation exchange. With the increase of $Pb^{2+}$ concentration, the ion exchange reaction becomes more adequate. The cations after the exchange reaction enter into the free water (Fig.8), and transport under the action of permeability. The measured concentration of cations ($Na^+$, $K^+$, $Ca^{2+}$, $Mg^{2+}$) in the leachate increases with the increase of $Pb^{2+}$ concentration, as shown in Fig.16. On the other hand, $Ca(HCO_3)_2$ and $Mg(HCO_3)_2$ are leached as dolomite hydrolyzes during the permeability test (see Eq. (11)), and $Ca^{2+}$ and $Mg^{2+}$ are released in their dissolution process (see Eqs.(12) and (13)). However, $Ca^{2+}$ can react with dolomite again, and $Mg^{2+}$ is released, then $CaCO_3$ precipitates, also called “dedomitization” (see Eq. (14)).

$$CaMg(CO_3)_2+2H_2O+2CO_2\longrightarrow Ca(HCO_3)_2+Mg(HCO_3)_2 \quad (11)$$

$$Ca(HCO_3)_2\longrightarrow Ca^{2+}+2HCO_3^- \quad (12)$$

$$Mg(HCO_3)_2\longrightarrow Mg^{2+}+2HCO_3^- \quad (13)$$

$$CaMg(CO_3)_2+Ca^{2+}\longrightarrow Mg^{2+}+2CaCO_3(s) \quad (14)$$

In addition, $CaCO_3$ is converted into $PbCO_3$ due to its high solubility under the $Pb^{2+}$ action, then the micro pores will be blocked by $PbCO_3$. Some $H^+$ is released due to the adsorption of $Pb^{2+}$ (see Eq.(8)). The cementation between particles is destroyed due to the corrosion of $H^+$, resulting in an increase in meso pore content and a deterioration of the microstructure.

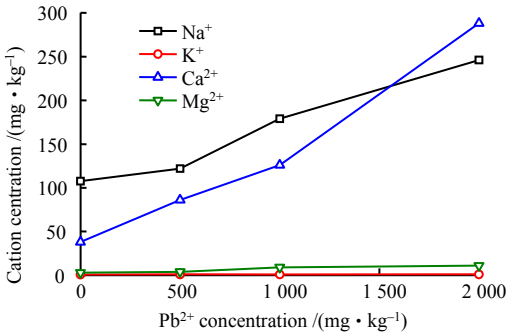


**Fig. 16 Variations of cation concentrations in leachate against $Pb^{2+}$ concentrations**

## 4 Conclusions

In this paper, the multi-step overflow method is used to investigate the water retention ability and permeability of Pb-contaminated loess based on VG model and CCG model. The internal mechanisms of the water retention ability and permeability caused by heavy metals are analyzed from a microscopic perspective by SEM, MIP and XRD tests. The main conclusions are as follows:

(1) The soil-water characteristic curve of Pb-contaminated compacted loess shifts downward with the increase of $Pb^{2+}$ concentration. The air-entry value of Pb-contaminated loess decreases with the increase of $Pb^{2+}$ concentration. When the $Pb^{2+}$ concentration increases from 0 mg/kg to 500, 1 000, and 2 000 mg/kg, the air-entry value decreases from 19.18 kPa to 16.24, 12.75, and 12.12 kPa, and lead contamination contributes to the reduction of water retention ability of loess.

(2) The saturated permeability coefficient increases from $7.92\times10^{-8}$ m/s to $3.73\times10^{-7}$ m/s as the lead concentration increases from 0 mg/kg to 2 000 mg/kg. With the help of VG model and CCG model, it is predicted that the unsaturated permeability coefficient of Pb-contaminated loess increases with lead concentration, while it decreases with the increase of matric suction, and the decrease rate increases with $Pb^{2+}$ concentration.

(3) The physical and chemical reactions between lead and soil particles cause the disintegration and transformation of minerals, which reduces the diffraction peak intensity of main minerals in loess. When the lead concentration increases from 0 mg/kg to 2 000 mg/kg, the negative potential on soil particle surface decreases from –15.7 mV to –11.2 mV. The cations in the diffuse double layer react with the lead ion, which changes the ion valence and ion concentration in the diffuse double layer, resulting in flocculation due to a decrease in the thickness of the diffuse double layer. The pore structure of the soil evolves from small pore to meso pore, and the intergranular pore size increases from 11.323 μm to 12.933 μm, then thus the macro water retention ability and permeability vary.

The results in this paper can provide important parameters for investigating unsaturated seepage and

solute transport in heavy metal contaminated sites, and it can provide useful reference for the engineering construction and treatment of heavy metal contaminated sites.

## References

[1] CHEN Yun-min. A fundamental theory of environmental geotechnics and its application[J]. Chinese Journal of Geotechnical Engineering, 2014, 36(1): 1–46.

[2] LI J S, XUE Q, WANG P, et al. Effect of lead (II) on the mechanical behavior and microstructure development of a Chinese clay[J]. Applied Clay Science, 2015, 105: 192–199.

[3] ZHANG Zhi-hong, LI Hong-yan, SHI Yu-min. Experimental study on permeability properties and micro-structure of clay contaminated by $Cu^{2+}$[J]. China Civil Engineering Journal, 2014, 47(12): 122–129.

[4] ZHA F S, ZHU F H, XU L, et al. Laboratory study of strength, leaching, and electrical resistivity characteristics of heavy-metal contaminated soil[J]. Environmental Earth Sciences, 2021, 80(5): 184.

[5] DUTTA J, MISHRA A K. Influence of the presence of heavy metals on the behaviour of bentonites[J]. Environmental Earth Sciences, 2016, 75(11): 1–10.

[6] LU Ning, LIKOS W, WEI Chang-fu, et al. Unsaturated soil mechanics[M]. Beijing: Higher Education Press, 2012.

[7] TAO Gao-liang, WU Xiao-kang, GAN Shi-chao, et al. Experimental study and model prediction of permeability coefficient of unsaturated clay with different initial void ratios[J]. Rock and Soil Mechanics, 2019, 40(5): 1761–1777.

[8] SIMMS P H, YANFUL E K. Measurement and estimation of pore shrinkage and pore distribution in a clayey till during soil-water characteristic curve tests[J]. Canadian Geotechnical Journal, 2001, 38(4):741–754.

[9] FEI Suo-zhu, TAN Xiao-hui, DONG Xiao-le, et al. Prediction of soil-water characteristic curve based on pore size distribution of soils[J]. Chinese Journal of Geotechnical Engineering, 2021, 43(9): 1691–1699.

[10] SUN Yin-lei, TANG Lian-sheng, LIU Jie. Advances in research on microstructure and intergranular suction of unsaturated soils[J]. Rock and Soil Mechanics, 2020, 41(4): 1095–1122.

[11] QI Dao-kun, PAN Yan-min, ZHANG Liang. Influence of microstructure on soil-water characteristic curve of undisturbed expansive soils[J]. Journal of Yangtze River Scientific Research Institute, 2019, 36(4): 145–150.

[12] LI Hua, LI Tong-lu, JIANG Rui-jun, et al. Measurement of unsaturated permeability curve using filter paper method[J]. Rock and Soil Mechanics, 2020, 41(3): 895–904.

[13] LI Ping, LI Tong-lu, WANG Hong, et al. Soil-water characteristic curve and permeability prediction on Childs & Collis-Geroge model of unsaturated loess[J]. Rock and Soil Mechanics, 2013, 34(Suppl.2): 184–189.

[14] ZHANG Deng-fei, CHEN Cun-li, YANG Jiong, et al. Deformation and water retention behaviour of collapsible loess during wetting under lateral confinement[J]. Chinese Journal of Rock Mechanics and Engineering, 2016, 35(3): 604–612.

[15] Ministry of Water Resources of the People's Republic of China. GB/T 50123－2019 Standard for geotechnical testing method[S]. Beijing: China Planning Press, 2019.

[16] ASTM. D 2487－11 Standard practice for classification of soils for engineering purposes[S]. West Conshohocken: PA: ASTM, 2017.

[17] PAREJA-CARRERA J, MATEO R, RODRÍGUEZ-ESTIVAL J. Lead (Pb) in sheep exposed to mining pollution: implications for animal and human health[J]. Ecotoxicology and Environmental Safety, 2014, 108(10): 210–216.

[18] ZHANG D F, WANG J D, CHEN C L. Gas and liquid permeability in the variably saturated compacted loess used as an earthen final cover material in landfills[J]. Waste Management, 2020, 105(11): 49–60.

[19] GARDNER W R. Calculation of capillary conductivity from pressure plate outflow data[J]. Soil Science Society of America Journal, 1956, 20(3): 317–320.

[20] FREDLUND D G, XING A. Equations for the soil-water characteristic curve[J]. Canadian Geotechnical Journal, 1994, 31(3): 521–532.

[21] VAN GENUCHTEN M T. A closed form equation for predicting the hydraulic conductivity of unsaturated soils[J]. Soil Science Society of America Journal, 1980, 44(5): 892–898.

[22] XIE Ding-yi. Soil mechanics for unsaturated soils[M]. Beijing: Higher Education Press, 2015.

[23] HU Zai-qiang, LIANG Zhi-chao, GUO Jing, et al. Prediction of permeability coefficient of unsaturated lime-improved loess[J]. Chinese Journal of Geotechnical Engineering, 2020, 42(Suppl.2): 26–31.

[24] CAI Guo-qing, HAN Bo-wen, YANG Yu, et al.

Experimental study on soil-water characteristic curves of sandy loess[J]. Chinese Journal of Geotechnical Engineering, 2020, 42(Suppl.1): 11–15.

[25] NEGAHDAR A, NIKGHALBPOUR M. Geotechnical properties of sandy clayey soil contaminated with lead and zinc[J]. SN Applied Sciences, 2020, 2(8): 1331.

[26] LEI Xiang-yi. The types of loess pores in China and their relationship with collapsibility[J]. Science China B, 1987, 17(12): 1309–1318.

[27] WU H, HU L M. Microfabric change of electro-osmotic stabilized bentonite[J]. Applied Clay Science, 2014, 101: 503–509.

[28] LI Z, TANG X, CHEN Y, et al. Sorption behavior and mechanism of Pb(II) on Chinese loess[J]. Journal of Environmental Engineering, 2009, 135(1): 58–67.

[29] WANG Y Z, CHEN Y, XIE H, et al. Lead adsorption and transport in loess-amended soil-bentonite cut-off wall[J]. Engineering Geology, 2016, 215: 69–80.